Short and Intermediate Range Order in Poly(alkylene oxide)s. A Neutron Diffraction and Molecular Dynamics Simulation Study

ARTICLE *in* MACROMOLECULES · SEPTEMBER 2012

Impact Factor: 5.8 · DOI: 10.1021/ma301197y

8 AUTHORS, INCLUDING:

Martin Brodeck
Forschungszentrum Jülich
11 PUBLICATIONS **124** CITATIONS
SEE PROFILE

Yixi Su
Forschungszentrum Jülich
121 PUBLICATIONS **1,381** CITATIONS
SEE PROFILE

Arantxa Arbe
Universidad del País Vasco / Euskal Herriko U…
128 PUBLICATIONS **2,759** CITATIONS
SEE PROFILE

Juan Colmenero
Universidad del País Vasco / Euskal Herriko U…
401 PUBLICATIONS **8,521** CITATIONS
SEE PROFILE

Macromolecules

Article

pubs.acs.org/Macromolecules

Short and Intermediate Range Order in Poly(alkylene oxide)s. A Neutron Diffraction and Molecular Dynamics Simulation Study

C. Gerstl,[†,‡] M. Brodeck,[†] G. J. Schneider,*[,‡] Y. Su,[‡] J. Allgaier,[†] A. Arbe,*[,§] J. Colmenero,[§,⊥,∥] and D. Richter[†,‡]

[†]Jülich Center for Neutron Science and Institut for Complex Systems, Forschungszentrum Jülich GmbH, D−52425 Jülich, Germany

[‡]Jülich Center for Neutron Science, Outstation at FRM II, 85747 Garching, Germany

[§]Centro de Física de Materiales (CSIC-UPV/EHU) and Materials Physics Center MPC, Paseo Manuel de Lardizabal 5, E-20018 San Sebastián, Spain

[⊥]Departamento de Física de Materiales (UPV/EHU), Apartado 1072, 20080 San Sebastián, Spain

[∥]Donostia International Physics Center, Paseo Manuel de Lardizabal 4, 20018 San Sebastián, Spain

ABSTRACT: Combining neutron diffraction with polarization analysis on isotopically labeled samples and fully atomistic molecular dynamics simulations, we have unravelled the structural features of the poly(alkylene oxide)s (PAOs) series. The experimental results show clear signatures of nanosegregation of main chains and side groups leading to the presence of alkyl nanodomains, as previously reported for other comb-like polymers like poly(*n*-alkyl methacrylates) (PnMAs). Comparison with polyethylene (PE) data shows that the atomic arrangements of side groups within the nanodomains in PAOs are more similar to bulk PE than those in PnMAs. After validating the simulations by direct comparison with the diffraction results on deuterated and protonated samples, we have exploited them to unveil the origin of the structure factor peaks and predict the outcome of potential neutron diffraction experiments on partially labeled samples. The simulated structures undoubtedly confirm the nanosegregation scenario in PAOs.

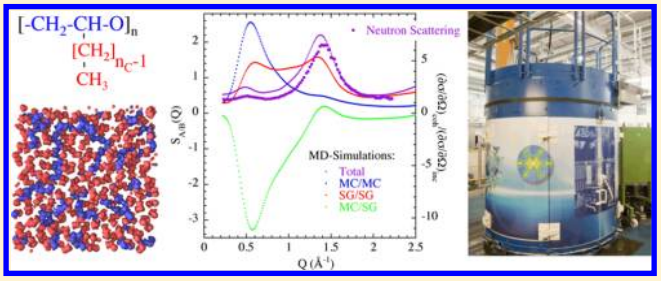

INTRODUCTION

In general, the local structure of soft materials is still poorly known. In diffraction experiments on polymers, this local structure emerges in the *Q*-range approximately $Q > 0.5$ Å^{-1}, where the patterns show two or more broad peaks, sometimes with shoulders. In the case of main-chain polymers without side groups, like polyethylene (PE), poly(ethylene oxide) (PEO), and 1,4-polybutadiene (PB), a main peak is observed centered at about 1.5 Å^{-1} and a weaker maximum is visible at around 3 Å^{-1}. The origin of these two peaks is usually deduced from qualitative arguments and taking into account their temperature dependence. The low-Q peak shifts with temperature, and therefore, it is generally attributed to intermolecular correlations, i.e., correlations between pairs of atoms belonging to different chains, governed by van der Waals interactions. The peak at higher *Q*-values does not depend on temperature and corresponds to rather small length scales. These observations lead to attribute it to intramolecular correlations, i.e., correlations between pairs of atoms belonging to the same chain and bonded via convalent bonds.[1] The patterns become more complex when polymers with side groups are considered, showing additional peaks and shoulders (see, e.g., ref 2). Similar qualitative analyses are used to determine their predominantly inter- or intramolecular origin, but almost nothing is known in most cases about the particular atomic or molecular correlations contributing to these peaks, i.e., about the actual short-range order in the real space.

Local structure of polymer systems has been traditionally investigated by means of X-ray diffraction which delivers only one partial structure factor. Neutron diffraction combined with selective deuteration allows to access different partial structure factors including—in the case of fully deuterated samples—the actual (total) structure factor $S(Q)$, where all the atoms are equally weighted. The problem for obtaining the coherent contribution to the diffraction patterns is the high level of incoherent scattering from the hydrogen atoms in protonated or partially protonated samples. Polarization analysis allows overcoming this difficulty since it nicely separates coherent and incoherent contributions. In this way, the combination of diffraction results on different partial structure factors has facilitated in some cases unraveling the short-range order in polymer melts.[3,4] However, the most powerful tool to decipher local structures in polymers is a critically validated fully atomistic molecular dynamics (MD) simulation. The information provided by diffraction experiments on differently labeled samples constitutes a demanding check to ensure the realism of

Received: June 13, 2012
Revised: August 14, 2012
Published: August 28, 2012

Table 1. Number of Alkyl Carbons in the Side-Group, Molecular Weight M_n, Polydispersity M_w/M_n, Density ρ (T given in °C), and Monomeric Coherent and Incoherent Scattering Cross Sections of the Samples Investigated

sample	n_C	M_n(g/mol)	M_w/M_n	ρ(g/cm^3)	σ^i_{coh} (barn)	σ^i_{inc} (barn)
h-PBO	2	10 200	1.04	$1.181-7.2\times10^{-4}T$	40.49	642.084
h-PHO	4	9380	1.03	$1.130-6.9\times10^{-4}T$	58.62	963.126
h-POO	6	9570	1.05	$1.102-6.6\times10^{-4}T$	76.749	1284.166
h-PDO	10	9340	1.03	$1.073-6.26\times10^{-4}T$	113.007	1926.252
d-PBO	2	39 800	1.04	$1.312-7.2\times10^{-4}T$	71.172	16.404
d-PHO	4	36 800	1.03	$1.266-6.9\times10^{-4}T$	104.642	24.606
d-POO	6	11 900	1.02	$1.240-6.6\times10^{-4}T$	138.112	32.806

the simulated structure, that can be subsequently scrutinized directly from the simulated atomic trajectories. This strategy has proved to be highly successful in several polymer systems.[2,5−10]

Over the last years, particular interest has been focused on the structural and dynamical features of the family on poly(*n*-alkyl methacrylates) (PnMAs) and other polymers containing alkyl side groups.[3,11−35] The main reason is the suggested formation of nanodomain structures by self-assembly of the side groups, that are segregated at nanometric scale from the main-chain subsytems. Such a morphology was deduced from the presence in the X-ray diffraction patterns of peaks at relatively low *Q*-values ("intermediate"-range), with side-group length dependent positions.[22,26,34] Later, neutron diffraction combined with isotopic labeling definitely proved such a scenario.[30,31] In addition, interesting confinement effects on the dynamics of the side groups have been reported,[26,30,31] in principle attributed to confinement effects induced by the surrounding main chains.

In this framework, recently the family of poly(alkylene oxides) (PAOs) has been subject of a series of systematic investigations including structural and dynamical aspects. From a structural point of view, the reported results[36] concern the unperturbed chain dimensions as investigated by small-angle neutron scattering (SANS). Interestingly, significant differences were found with respect to analogous poly(olefine)s with the similarly long alkyl side groups. However, the short/intermediate range spatial order and the possible formation of alkyl nanodomains in PAOs were not addressed until now. The dynamics have been investigated by dielectric and mechanical spectroscopies[37] as well as by quasielastic neutron scattering.[38] For these polymers, the side groups motions did not show anomalies attributable to confinement effects. If such effects emerged as a consequence of the nanosegregation of side groups and main chains, the question arises: Is the nanosegregation suppressed in PAOs by the large flexibility of the PEO-like main chain? A recent computational investigation[39] of a simple bead−spring model for comb-like polymers mimicking polymers with long side groups like PAOs or PnMAs has shown that nanosegregation of main chains and side groups can arise as a purely entropic effect, provided that the density of branch points is large enough. Thus, PAOs could contradict this universal prediction from the simulations. Unveiling the structural features of this family of polymers is thus mandatory.

With these ideas in mind, we have performed a combined approach including neutron diffraction and MD-simulations to determine the structure of PAOs at short and intermediate (from angstroms to a few nanometers) length scales. Fully deuterated and fully protonated samples with different side-group lengths (2, 4, 6, and 10 alkyl carbons) have been investigated by neutron diffraction with polarization analysis, providing the total and a partial structure factor. We have found clear experimental evidence for the presence of alkyl nanodomains within which the local structure is even more similar to bulk PE than in the case of PnMAs. Moreover, the properly validated simulated samples (with two and four alkyl carbons) have provided direct proof of the nanosegregation and allowed calculating different magnitudes like the contributions of the main molecular groups (main chains and side groups) to the structure factor or the expected results of neutron diffraction on partially deuterated samples.

EXPERIMENTAL SECTION

Samples. We have investigated poly(alkylene oxide)s (PAO's) with increasing number of alkyl carbons along the side groups (n_C) (see Table 1 and chemical formulas in Figure 1). Both, fully protonated (h-PAOs) and fully deuterated (d-PAOs) were studied, except for the case n_C = 10, where only h-PDO was available. The samples were synthesized at the Forschungszentrum Jülich by anionic ring-opening polymerization[36,37,40] and show the characteristics displayed in Table 1. In the case of a poly(propylene oxide) sample polymerized under the same reaction conditions the stereochemistry was found to be atactic. DSC measurements revealed glass-transition temperatures T_g within the interval 205 ± 1 K for all the samples. Crystallization occurs at T_C = 247 and 290 K for POO and PDO, respectively (heating rate of 20 K/min). Their melting temperatures are T_M = 248 K (POO) and 295 K (PDO).

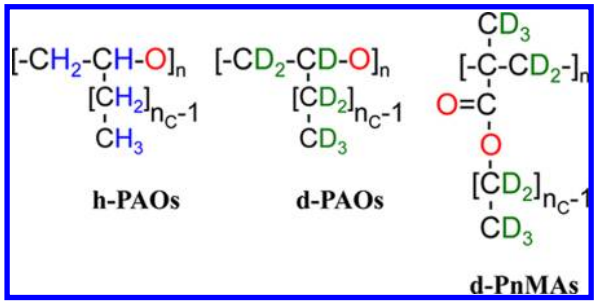

Figure 1. Chemical formulas of the PAOs investigated in this work. That of deuterated PnMAs is also shown for comparison.

Neutron Scattering. Neutron diffraction measures differential scattering cross sections, i.e., the number of neutrons scattered into a solid angle comprised between Ω and Ω + dΩ with respect to the total number of incident neutrons.[41−44] The differential scattering cross section contains a coherent and an incoherent term. The coherent part is related to the relative position of pairs of atoms giving information on the structural organization of the sample:

$$\left(\frac{\partial\sigma}{\partial\Omega}\right)_{coh} = \frac{1}{N}\langle\sum_{i,j=1}^{N}\bar{b}_i\bar{b}_j e^{i\vec{Q}\vec{r}_{ij}}\rangle \quad (1)$$

Here b_i is the neutron scattering length of nucleus i, N is the number of atoms, $\vec{r}_{ij} = \vec{r}_i - \vec{r}_j$ is the vector difference between atoms i and j and

dx.doi.org/10.1021/ma301197y | Macromolecules 2012, 45, 7293−7303

the brackets express the thermal average. In the limit $Q \rightarrow \infty$, the differential coherent cross section is determined by the total coherent cross section σ_{coh}:

$$\left(\frac{\partial\sigma}{\partial\Omega}\right)_{coh} = \frac{1}{N}\sum_{i=1}^{N}\overline{b_i}^2 = \frac{1}{4\pi N}\sum_{i=1}^{N}\sigma_{coh}^i = \frac{\sigma_{coh}}{4\pi} \quad (2)$$

The incoherent contribution is related to the fluctuations of scattering lengths in the sample. It is Q-independent and determined by the total incoherent cross section σ_{inc}:

$$\left(\frac{\partial\sigma}{\partial\Omega}\right)_{inc} = \frac{1}{N}\sum_{i=1}^{N}\overline{\Delta b_i^2} = \frac{1}{4\pi N}\sum_{i=1}^{N}\sigma_{inc}^i = \frac{\sigma_{inc}}{4\pi} \quad (3)$$

The values of the scattering lengths, coherent and incoherent scattering cross sections of the different atoms composing the samples here investigated are reported in Table 2. The cross sections of the polymers can be found in Table 1.

Table 2. Values of the Average Scattering Lengths $\overline{b_i}$, Coherent ($\sigma_{coh}^i = 4\pi\overline{b_i}^2$), and Incoherent ($\sigma_{inc}^i = 4\pi\overline{\Delta b_i^2}$) Cross Sections for the Isotopes i Composing the Samples Investigated

isotope i	$\overline{b_i}$/fm	σ_{coh}^i/barn	σ_{inc}^i/barn
^{1}H	−3.7406	1.7583	80.27
^{2}H (D)	6.6710	5.592	2.05
^{12}C	6.6511	5.559	0
^{16}O	5.8030	4.232	0

In order to separate the coherent and incoherent differential scattering cross sections and extract information on the local structure, we performed diffraction experiments with polarization analysis (see for example[45,46]). If the incoherent scattering is only generated by spin disorder, the spin of the neutrons is flipped with a probability 2/3 by incoherent scattering, while no spin-flip is observed for coherent scattering. Therefore, if the incident neutron beam is polarized, the number of spin-flipped (SF) and non spin-flipped (NSF) neutrons detected under a certain solid angle is given by:

$$I_{SF} = I_0\frac{2}{3}\left(\frac{\partial\sigma}{\partial\Omega}\right)_{inc} \quad (4)$$

$$I_{NSF} = I_0\left[\left(\frac{\partial\sigma}{\partial\Omega}\right)_{coh} + \frac{1}{3}\left(\frac{\partial\sigma}{\partial\Omega}\right)_{inc}\right] \quad (5)$$

From the SF measurement the quantity I_0, which depends on the sample volume, incident intensity, detector efficiencies, etc., can be determined. With this information, the coherent differential cross section in absolute units can be extracted from the NSF measurement. From the values I_{SF} and I_{NSF} obtained after correcting the measured intensity with the finite flipping ratio, the ratio between the coherent and incoherent scattering cross sections can also easily be calculated:

$$\frac{\left(\frac{\partial\sigma}{\partial\Omega}\right)_{coh}(Q)}{\left(\frac{\partial\sigma}{\partial\Omega}\right)_{inc}(Q)} = \frac{I_{NSF}(Q) - \frac{1}{2}I_{SF}(Q)}{\frac{3}{2}I_{SF}(Q)} \quad (6)$$

This procedure has the advantage that the delivered magnitude is directly corrected for Debye−Waller factor and instrumental effects. Since the degree of deuteration is usually not known with high accuracy, the cross sections are not in absolute values.

Diffraction Measurements. The neutron diffraction experiments with polarization analysis were performed at the DNS instrument of JCNS located at the Forschungsreaktor FRM-II in Garching (Germany). With an incident wavelength of 4.74 Å and an angular scattering range from 5° to 125°, the Q-range from 0.23 to 2.0 Å^{-1} was covered.

Flat aluminum sampleholders sealed with Indium were used. The deuterated samples were investigated at 170, 200, 230, 260 K and room temperature (RT ≈ 300 K), while h-PAOs only at RT. A standard top-loading cryostat was used to cool the samples to low temperatures. The thicknesses (0.7 mm for d-PAOs and 0.2 mm for h-PAOs) were chosen to deliver a similar transmission for both kinds of samples. The background was measured on an empty cell and subtracted by applying the corresponding transmission-dependent corrections. In order to avoid artifacts from the orientation of the sample, measurements at 45° and 135° with respect to the incident beam were preformed and subsequently averaged. Measuring times varied from 1.7 h on d-PAOs to 7.5 h on h-PAOs.

For comparison, a fully deuterated polyethylene sample (d-PE) was investigated at 150, 175, 200, 225, 245, 275, and 300 K. To reduce crystallization a molten sample was quenched by immersion in liquid nitrogen before the experiment.

MOLECULAR DYNAMICS SIMULATIONS

The simulations were carried out using Materials Studio 4.1 and the Discover-3 module (version 2005.1) from Accelrys with the condensed-phase optimized molecular potentials for atomistic simulation studies forcefield (COMPASS). The simulated systems were built by means of the well-known amorphous cell protocol, which was proposed for the first time by Theodorou and Suter.[47,48] The polymers simulated were PBO and PHO. For each case, a cubic cell containing ten polymer chains of 80 monomer units each under periodic boundary conditions was constructed. Standard minimization procedures (Polak−Ribiére conjugated gradients method) were followed in order to minimize the so obtained energy structure. The system was then simulated at very high temperatures to cause a significant mixture of the chains within the simulation cell. Afterward, the temperature was lowered to 360 K and the whole system was equilibrated for 10 ns. The cell dimensions were $(38)^3$ Å^3 (PBO) and $(53)^3$ Å^3 (PHO), fixing the densities to the corresponding experimental values at this temperature (Table 1).

Although the COMPASS forcefield is able to parametrize deuterium atoms, we have rather decided to simulate fully protonated samples in all cases. For the following comparison with deuterated experimental data we have simply used the different scattering lengths for the corresponding isotopes. The justification of this is based on the fact that such a procedure has yielded good agreements in the past among simulations of different polymeric systems, obtained by means of a forcefield (PCFF), without an explicit dynamic parametrization for deuterium atoms. Moreover, we have checked within the COMPASS forcefield that the difference in structure data is nonexistent when using explicit deuterium atoms and very small and restricted to the fastest available time values for the dynamic data.

EXPERIMENTAL RESULTS AND COMPARISON WITH OTHER SYSTEMS: SCENARIO OF NANO-SEGREGATION

Diffraction Results on PAOs. Figure 2 displays the DNS results on the deuterated samples. Since the values of the average scattering length of all isotopes in these samples are almost identical (Table 2), all the correlations are equally weighted in eq 1 and neutron diffraction reveals the true or total structure factor $S(Q)$.

Let us first focus on the d-PHO results (Figure 2b). A main peak (let us call it peak II) is observed centered at around Q_{II} = 1.5 Å^{-1}, that shifts toward lower Q-values with increasing temperature. The shift is less pronounced in the glassy state (two lowest temperatures investigated). These are the typical features of the first amorphous halo revealing intermolecular correlations in glass-forming polymers (see, e.g., ref 1). In addition, a much weaker "prepeak" is found at lower Q-values, around ≈0.5 Å^{-1}. The position of this peak (we will call it peak

dx.doi.org/10.1021/ma301197y | Macromolecules 2012, 45, 7293−7303

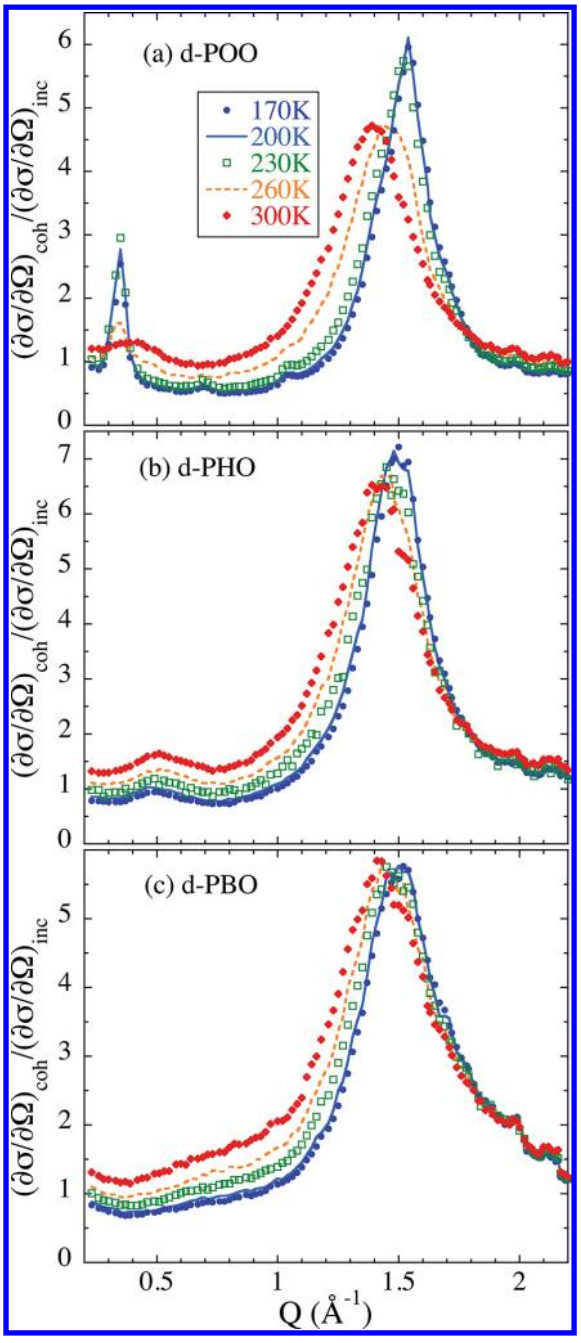

Figure 2. Ratio between coherent and incoherent differential cross sections measured on the fully deuterated samples: (a) d-POO; (b) d-PHO; (c) d-PBO. The temperature code is shown in part a.

I) is independent of temperature, but the intensity increases when the sample is heated.

The general features described for the structure factor of d-PHO are extensible to those of d-PBO and d-POO (in the latter case, for the $T \leq 260$ K results). The position of the main peak Q_{II} is essentially the same in the three samples. Peak I—hardly visible in PBO—shifts toward lower Q-values with increasing side-group length. On the other hand, the d-POO sample shows clear signs of the presence of crystallinity at low temperatures, that manifest in the emergence of sharp intense peaks at $Q \approx 0.34$ and 1.5 Å^{-1} and weaker narrow peaks in between.

In Figure 3, the results corresponding to the protonated samples at RT are displayed. The magnitude of the ratio

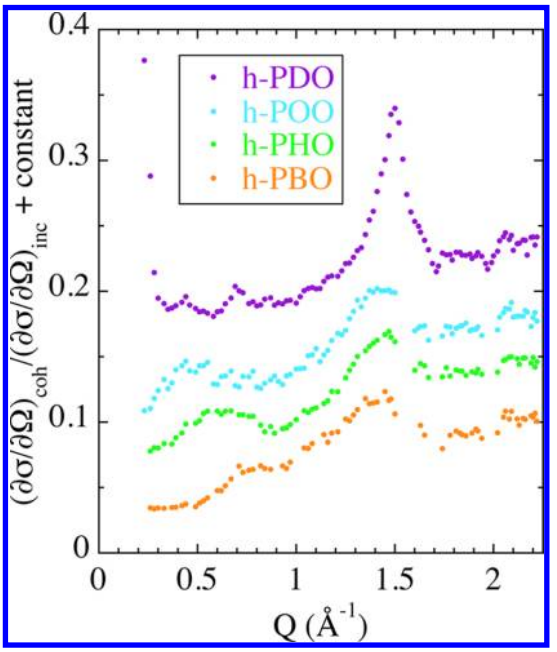

Figure 3. Ratio between coherent and incoherent differential cross sections measured on the fully hydrogenated samples at 300 K. A constant has been added [0.05 (h-PHO), 0.10 (h-POO), and 0.15 (h-PDO)] for a better visualization.

between coherently and incoherently scattered intensities is much smaller than in the case of the deuterated counterparts (compare Figure 2 and Figure 3 and Table 1), leading to a much worse statistics of the data despite the long measuring times. These results reveal differently weighted partial structure factors. The main difference with respect to the d-PAOs structure factor is that the correlations of pairs of atoms involving H and either C or O are negatively weighed (see Table 2). As a result, the relative intensity between peaks I and II becomes much larger. Apart from this, the main features of the patterns are rather similar (e.g., the positions of the peaks are very much the same in a given protonated sample and its deuterated counterpart). Figure 3 shows additional results on h-PDO, that clearly reveal crystallinity signatures (the melting point of this sample is very close to RT).

Comparison with PnMAs and PE: the Nano-Segregation Scenario. The interpretation of the origin of the peaks in the structure factors of PAOs can be facilitated taking into account their similarity with those of PnMAs, as shown in Figure 4. For PnMAs, it was suggested that side groups of different monomeric units tend to self-assemble in alkyl nanodomains [called polyethylene (PE)-like nanodomains] nanosegregated from the main chains.[22,26,34] By exploiting neutron selectivity for labeled molecular groups and comparing the diffraction data with those corresponding to bulk PE,[30] it was concluded that the main peak II arises from correlations between atoms located in side groups of different monomers in a PE-like environment. In this way, the existence of PE-like nanodomains in high order PnMAs was demonstrated, supporting the hypothesis of the nanosegregation.

We discuss now the possible extension of such interpretation of peak II for PAOs. For $n_c \leq 4$, crystallization is suppressed in PAOs and their alkyl nanodomains, if existing, would be

dx.doi.org/10.1021/ma301197y | Macromolecules 2012, 45, 7293−7303

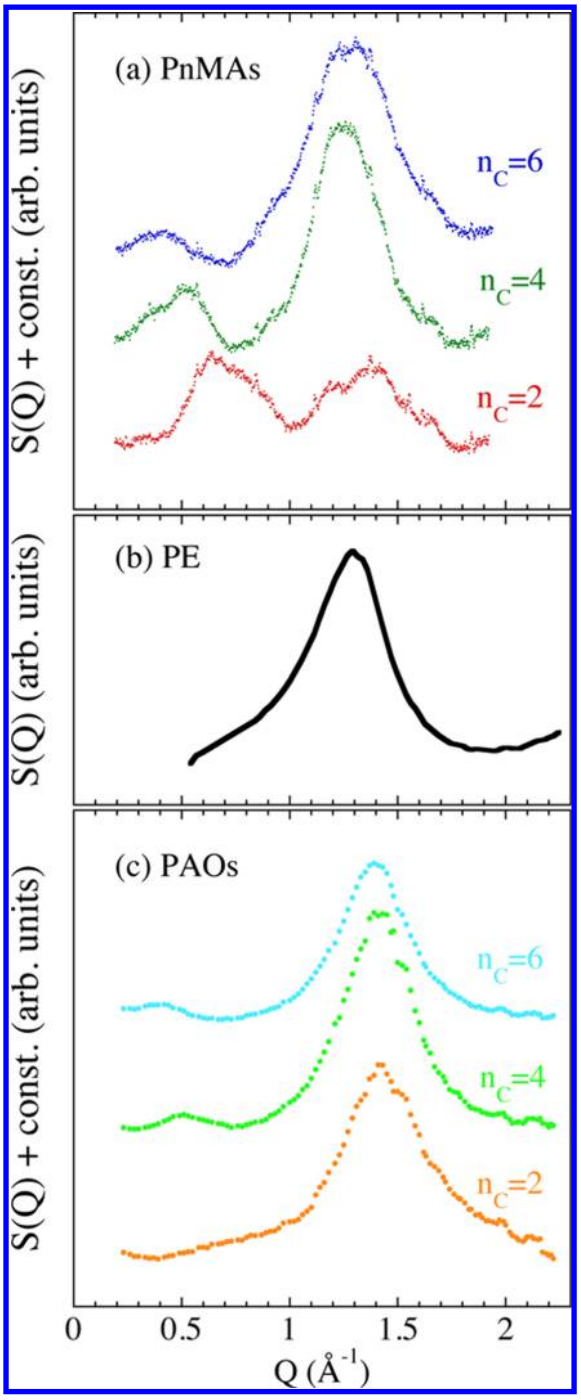

Figure 4. Static structure factor measured on fully deuterated samples of the families of PnMAs (a)[30] and PAOs (c) with different side-group lengths. Panel b shows as reference the structure factor of molten PE at 421 K. Data in part a correspond to a temperature about 75 K above the respective glass-transition temperatures, data in part c to 300 K. Shifts have been applied for a better visualization.

expected to present the features of amorphous PE. PE is semicrystalline below $T_M \approx 400$ K, and the data reported up to now on the intermolecular peak of PE correspond to a molten sample at $T \geq 420$ K.[49] Figure 4 illustrates the similarity of peak II in PAOs with the structure factor of molten PE at 421 K (Figure 4b). We note however the different positions of the maxima. This could be due to the different temperatures considered for the comparison. To obtain information on the amorphous PE peak in the temperature range here explored we performed diffraction measurements on a quenched d-PE sample. These data will also be valuable for a further comparison of the features in the semicrystalline d-POO sample. Figure 5 shows the results obtained in the Q-range

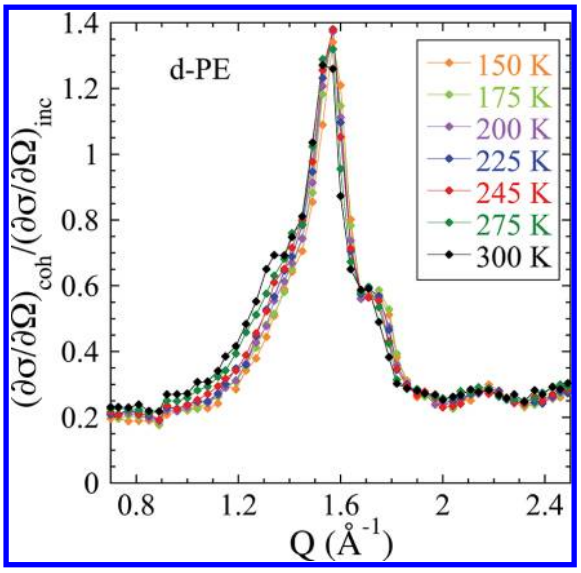

Figure 5. Ratio between coherent and incoherent differential cross sections measured on a fully deuterated PE sample at the temperatures indicated.

where the PE intermolecular correlations are expected to contribute. Clear crystallinity signatures are found (mainly the sharp peak centered at $Q^{PE}_{Xtal} \approx 1.56$ Å^{-1}), that prevent an accurate determination of the position of the peak associated with the amorphous fraction (which position will be referred to as Q^{PE}_{inter}). However, it is clear that the temperature dependence of the crystalline peak is much weaker than that of the intensity in the region 1.0−1.4 Å^{-1}. The shift of the pattern in this region is due to the expansion of the amorphous phase. To deduce the temperature dependence of the amorphous peak at 300 K and below, for any given temperature T we applied a shift in the Q-scale $\Delta Q^{PE}_{inter}(T)$, such that the pattern matches that of a reference temperature T_R (T_R = 245 K) the region 1.0...1.4 Å^{-1}. Assuming that above the glass-transition Q^{PE}_{inter} can be extrapolated from the data above the melting point, we determined $Q^{PE}_{inter}(T_R = 245\ K) = 1.43$ Å^{-1} and obtained the values at other temperatures as $Q^{PE}_{inter}(T) = Q^{PE}_{max}(245\ K) + \Delta Q^{PE}_{inter}(T)$. Figure 6 shows the such deduced values. We note the good agreement between the temperature dependence of the values for $T \geq 245\ K$ and that in the molten state, supporting the procedure followed. We have also represented the values of Q^{PE}_{Xtal}. The interchain distances in the crystalline phase are slightly reduced with respect to the average distances in the amorphous parts ($2\pi/Q^{PE}_{Xtal} \approx 4.0$ Å vs $2\pi/Q^{PE}_{inter} \approx$ 4.3...4.5 Å in the T-range from 150 to 300 K).

As can be seen in Figure 6, the position of peak II in PAOs practically coincides with that of Q^{PE}_{inter}, providing strong support to the proposed interpretation of peak II. The average intermolecular distances within the alkyl nanodomains in PAOs are thus almost identical to those in the amorphous phase of semicrystalline PE. Their temperature dependences are also very similar. Linear expansion coefficients of $\alpha^{PBO}_{peakII} = (5.3 \pm 3) \times 10^{-4}$ K^{-1} and $\alpha^{PHO}_{peakII} = (5.5 \pm 0.5) \times 10^{-4}$ K^{-1} are obtained in the T-range above 200 K. These values are higher

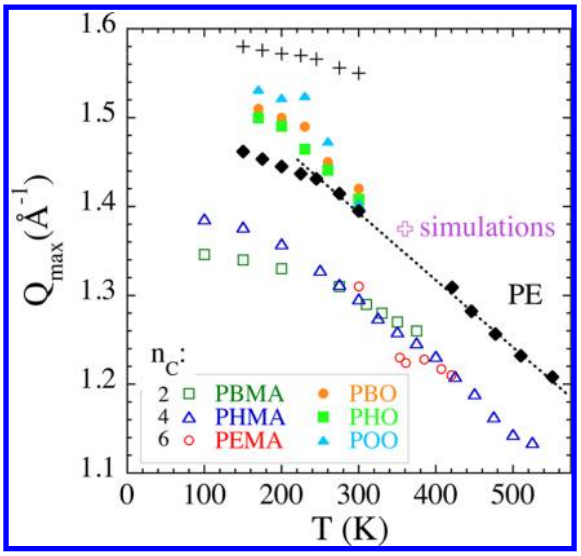

Figure 6. Temperature dependence of the position of the main peak of the structure factor in PAOs and PnMAs[4,31] (Q_{II}) with the same number of alkyl carbons. Data corresponding to the first amorphous halo (interchain correlation peak, Q_{inter}^{PE}) (black diamonds) and the main crystallinity peak (Q_{Xtal}^{PE}) (crosses) of PE[49] are also shown for comparison.

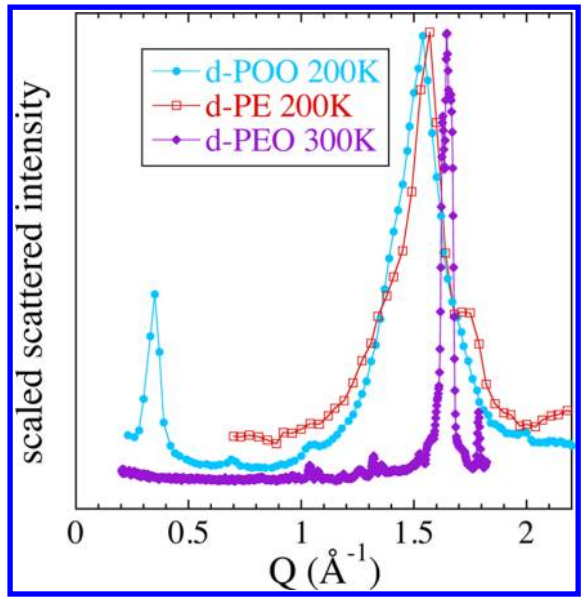

Figure 7. Intensities scattered by fully deuterated POO (d-POO), PEO (d-PEO) and PE (d-PE) in the solid state. They have been scaled to directly compare the different samples.

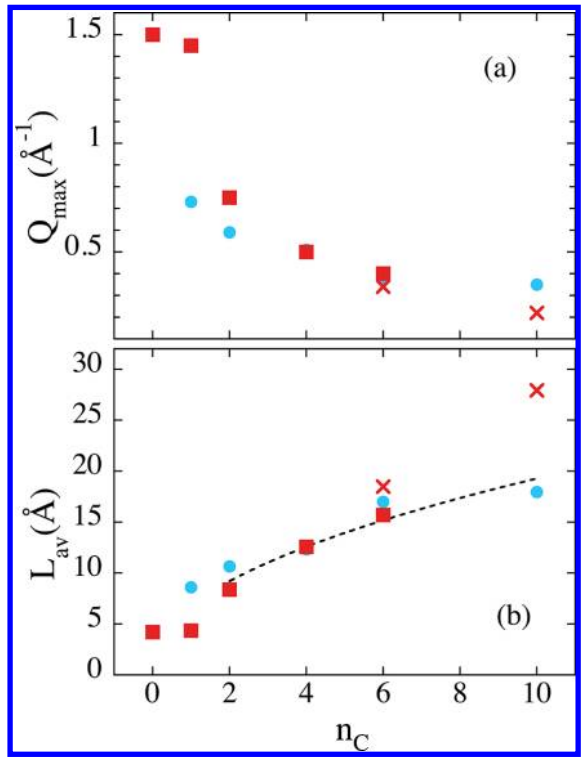

Figure 8. (a) Position of the low-Q maximum of the structure factor of PAOs (red filled squares) and PnMAs (blue filled circles) Q_I as a function of the number of alkyl side carbons. The crosses correspond to the sharp peaks arising in the crystalline phases of PAOs. The corresponding average distances in the Bragg approximation ($2\pi/Q$) are depicted in (b). Results corresponding to the main peaks of PPO at RT[50] and PEO at 363 K[51] are shown. An $n_C^{1/2}$-dependence (dashed line) could reasonably describe the data in the amorphous polymers; see text.

than those deduced from macroscopic density measurements (from Table 1, $\alpha_{macro}^{PBO} = 1.57 \times 10^{-4}$ K^{-1} and $\alpha_{macro}^{PHO} = 2.23 \times 10^{-4}$ K^{-1} can be deduced) (see below). Figure 6 also shows that the average distances associated with peak II appear to be slightly increased in PnMAs (4.5−4.9 Å below RT), reflecting a less compact structure within the nanodomains. Nevertheless, the expansion coefficients deduced for PnMAs from the position of peak II are very similar to that of PE and in PAOs and, like in the case of PAOs, significantly smaller than the macroscopically observed ones.[4]

At low temperatures the values of Q_{II}^{POO} are systematically higher than those of PHO and POO. This is probably due to the presence of the crystalline contribution. Figure 7 directly compares d-PE and d-POO structure factors below the melting. The striking similarity further supports the assignment of this peak to PE-like correlations. Note also that the comparison with the structure factor of crystalline PEO (see Figure 7) rules out contributions of crystallites involving stacking of neighboring main-chain segments to the structure factor of POO.

Moving now to peak I, from the neutron scattering investigations of labeled PnMAs samples it was concluded that this peak contains intermolecular correlations involving main-chain atoms.[30] Later, coarse-grained simulations on comb-like polymers[39] confirmed that this peak is characteristic for interdomain correlations. Thus, the peak position Q_I should be determined by the average nanodomain size, as previously suggested by other authors.[22,26,34] Figure 8a shows the n_C-dependence of Q_I for both, PAOs and PnMAs. We have also included the values reported for the main-peak positions of PPO[50] ($n_C = 1$) and PEO[51] ($n_C = 0$) above its melting temperature. The average characteristic distances obtained in the Bragg approximation ($L_{av} = 2\pi/Q_{max}$) are represented in Figure 8b. There is a clear increase of L_{av} with increasing side-group length, from 4 Å for the main-chain polymer PEO up to ≈16 Å for POO ($n_C = 6$). Compared with the corresponding values in PnMAs, L_{av} is similar for $n_C = 6$ and $n_C = 4$, independently of the nature of the main chain. The latter seems to play a role only for short side-group polymers; there, the relative volume occupied by the main chains is more important and leads to larger average distances between constituent

dx.doi.org/10.1021/ma301197y | Macromolecules 2012, 45, 7293−7303

subsystems (side groups and main chains) in acrylates than in oxides. We also note that while for PnMAs L_{av} increases monotonically with n_C, L_{av} in PAOs shows a rather abrupt step from $n_C \leq 1$ to $n_C \geq 2$. Apparently, the presence of one single methyl group in the PPO monomer leads only to a rather small increase of the average interchain distance with respect to PEO. This might be the consequence of a very effective packing due to the "stretched" trans conformation as deduced for PPO in ref 50. In that work, combining diffraction and reverse Monte Carlo simulation, it was found that two consecutive methyl groups are pointing in almost opposite directions. However, adding a further alkyl group in the side group induces a significant separation between adjacent chains. Such effect—the nanosegregation—seems to be well established for $n_C \geq 4$, leading to main-chain independent sizes of the nanodomains. The n_C-dependence of L_{av} in PAOs could in principle be well described by a linear increase. However, considering the case $n_C = 10$ in PnMAs, a tendency to saturation or a weaker dependence is observed for longer alkyl side groups. In the literature it has been proposed[18,22] that a $n_C^{1/2}$-dependence could apply, taking into account the Gaussian-coil conformation of polymers. This kind of law might be unrealistic for small chain segments as those in the side groups of our systems (the Kuhn length of PE is 14 Å). Nevertheless, the conformation of the side groups has to be less extended than in the all-trans configuration. As we show in the following, this can be deduced from the comparison with the results on the crystalline samples. We noted above the emergence of a sharp peak in the low-Q range of d-POO (see Figure 2a). This peak is located at 0.34 $Å^{-1}$, with associated distances of 18.5 Å and therefore difficult to assign to PE-lamellar structure (where typical interlamellar distances are of about 100 Å). In the scenario of the nanodomain structure, the sharp peak in POO's structure factor should be attributed to a well-defined correlation between main-chain portions of chains fixed by crystalline side groups arrangements (all-trans) in between. The induced separation is somewhat larger than that deduced for the amorphous system (see Figure 8), suggesting the coiling of side groups in the latter. Furthermore, higher (2nd and 3rd) order reflections are visible in the pattern, indicating a well-developed order. The results on h-PDO (Figure 3) also show indications of weak sharp peaks at ≈0.44 and 0.67 $Å^{-1}$ that could be interpreted as high-order peaks, corresponding to a main reflection at ≈0.22 $Å^{-1}$ outside the Q-range accessible at the DNS instrument. The steep increase of the intensity at low Q in Figure 3 corresponds to the high-Q flank of this peak. The associated distance between main chains in PDO would be markedly larger than that found on the amorphous PnMAs counterpart (see Figure 8).

For a given sample, the main influence of temperature on peak I is an increase in the intensity. It can be shown that the maxima can be scaled to a common temperature leading to a good superposition (except in the high-Q flank, due to contributions of peak II). The scaling factors display a linear dependence with temperature, according to the expected behavior of the low-Q limit of the density fluctuations (the coherent intensity is proportional to $T\beta$, being β the isothermal compressibility). Thus, as reported for PnMAs,[52] no appreciable change with temperature is observed for the peak I positions ($\alpha_{peakI} \approx 0$). If the linear expansion coefficient deduced from macroscopic density measurements α_{macro} results from an average of the expansion coefficients associated with peaks I and II, this finding could explain the above commented observation of smaller values for α_{macro} with respect to those obtained from the shifts of peak II. However, we indeed expect that α_{macro} would be ultimately determined by the thermal behavior of the nanodomain structures, i.e., by α_{peakI}, rather than by the expansion within them. We speculate that the finding of T-independent positions of peak I does not necessarily imply the insensitivity of the nanodomain structure to thermal variations. As we will see below, peak I contains different contributions, including even a strong anticorrelation between side-group and main-chain atoms. The intricated interplay between these different contributions may lead to counterintuitive behaviors.

SIMULATIONS: VALIDATION AND BEYOND

Simulations vs Experiments: Validation. From the atomic positions in the simulated cells, the magnitudes measured in the neutron diffraction experiments can be computed and directly compared with the experimental results. The outcome is displayed in Figure 9. To minimize finite-size effects we have restricted the Q-range considered to the region $Q \geq 2\pi/(L/2)$, where L is the lateral cell dimension (L = 38 Å for PBO and 53 Å for PHO). We observe an excellent agreement between both sets of results regarding the qualitative features of the patterns and no hints of spurious oscillations in the simulation data can be seen. However, some quantitative discrepancies are noticed. In the detailed comparison, a series of factors have to be taken into account: (i) The temperatures of simulated and real samples are not the same (360 K vs 300 K). This is expected to be the origin of the slight shifts toward lower Q-values of the simulated main peaks with respect to the real ones. The position of peak II as obtained from the simulations is plotted in Figure 6. It fits rather well with the overall experimental results, though for a perfect match a somewhat lower temperature should be assumed for the simulations (about 325−340 K instead of 360 K). (ii) The deuteration level of d-PAOs might not be exactly 100%. The presence of a tiny amount of protons drastically reduces the ratio between coherent and incoherent cross sections. Assuming proton amounts of about 1.3% for d-PBO and 0.7% for d-PHO—both within the uncertainties of the deuteration level of the samples—would be enough to match the intensities of the simulated curves. (iii) Despite the use of very thin protonated samples, due to their large incoherent cross sections multiple scattering contributions cannot discarded. Their main effect is expected to be a weakly Q-dependent additional component in the deduced coherent cross-section.[5] This would explain the differences between simulated and measured results in Figure 9, parts b and d. Thus, the discrepancies can be largely rationalized and from this demanding test we can conclude that for both samples the structure of the simulated cells very accurately reproduces that of the real samples. Once the reliability of the simulations is assured, they can be exploited to obtain information on magnitudes that are difficult or cannot be experimentally accessed.

Exploiting the Simulations. Simple visualization of the PHO cell in Figure 10 −obviously not possible experimentally− provides clear evidence of the presence of nanodomains. To gain quantitative insight into the structure, the atomic pair correlation functions contributing to the structure factor can be grouped according to the two molecular substructures conforming PAOs' monomers: the main chain (MC) and the side group (SG), see Figure 11. The partial structure factor

dx.doi.org/10.1021/ma301197y | Macromolecules 2012, 45, 7293−7303

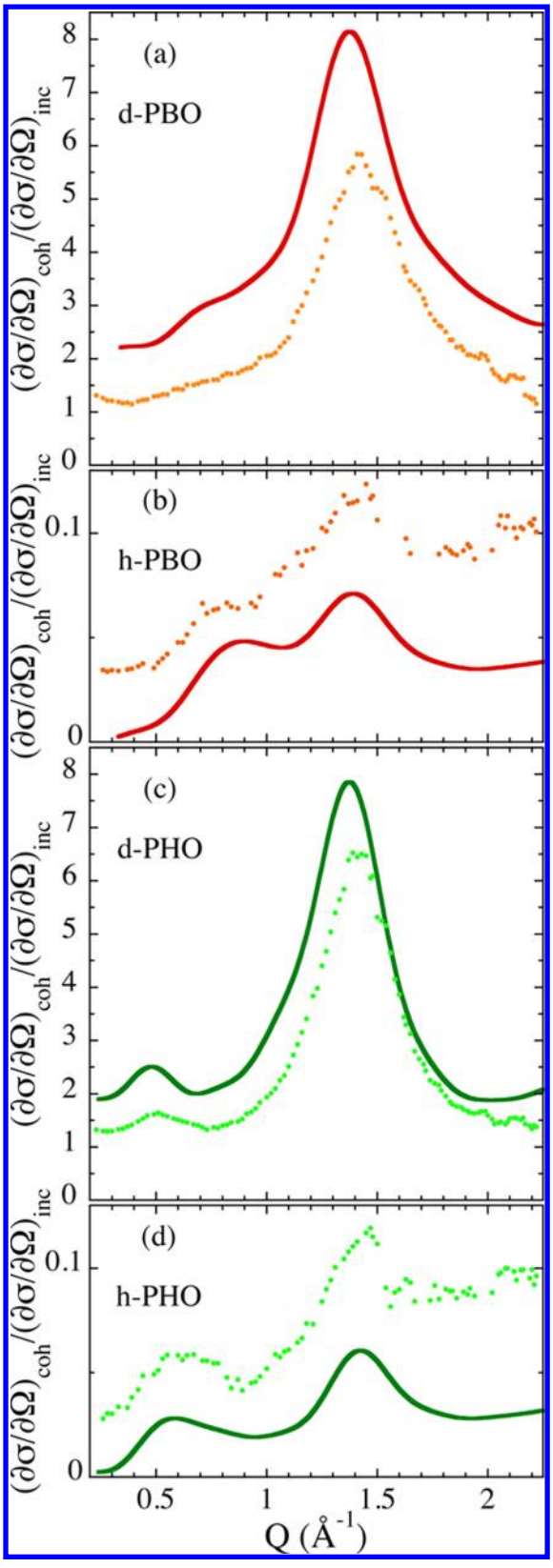

Figure 9. Direct comparison of the ratio between coherent and incoherent differential cross sections measured at 300 K and calculated from the simulations at 360 K for the fully deuterated PBO and PHO samples: (a) deuterated PBO; (b) protonated PBO; (c) deuterated PHO; (d) protonated PHO.

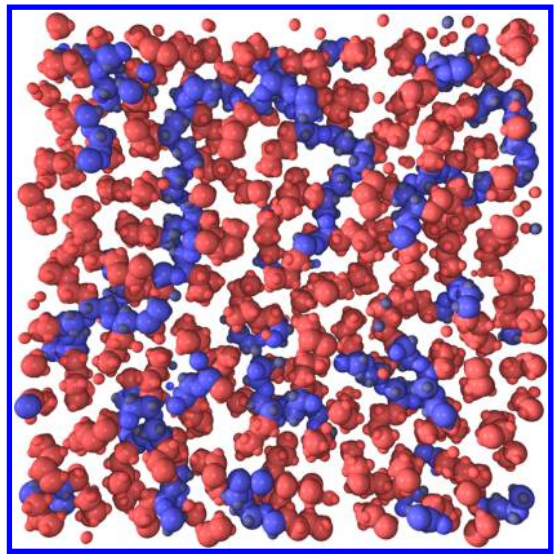

Figure 10. Slice of the simulation cell of PHO. Main-chain atoms are represented in blue, side-group atoms in red.

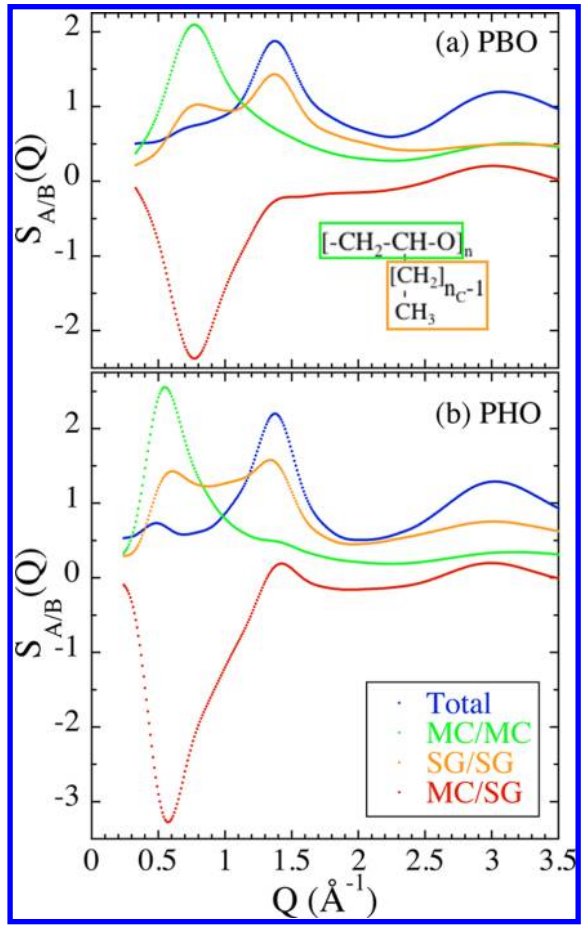

Figure 11. Contributions to the normalized total structure factors for PBO (a) and PHO (b) calculated from the MD-simulations. The definitions of MC and SG subsystems are shown in the scheme of the monomer in part a by the green and orange rectangles, respectively.

involving A/B correlations (where A and B can be either MC or SG) is calculated as:

dx.doi.org/10.1021/ma301197y | *Macromolecules* 2012, 45, 7293−7303

$$S_{A/B}(Q) = \frac{1}{N}\langle \sum_{i,j\in A,B}^{N_A,N_B} e^{i\vec{Q}\vec{r}_{ij}}\rangle \quad (7)$$

(i. e., eq 1 with all scattering lengths set to 1 and restricted to the desired subgroups of atoms). The results obtained are shown in Figure 11 together with the total structure factors [S_{total} $(Q) = \sum_{A,B} S_{A/B}(Q)$]. First of all we note that, as anticipated, the total structure factors are nearly identical to the experimentally accessed coherent cross sections in the fully deuterated samples. They reveal the presence of peaks I and II centered at Q_I and Q_{II} respectively, and, extending the Q-range under investigation toward higher values, a third peak at $Q_{III} \approx 3$ Å^{-1} is also observed that does not appreciably depend on the side-group length.

The basic features observed for the partial correlation functions are essentially the same for both polymers:

- The MC/MC correlations show a main peak centered at a position $Q_I^{MC/MC}$ (0.76 Å^{-1} for PBO, 0.54 Å^{-1} for PHO) close to that of the first peak of the total structure factor Q_I. A kind of shoulder is envisaged in the neighborhood of Q_{II} and a broad peak can be seen around Q_{III}. Thus, main chains show predominantly average distances among them of $2\pi/Q_I^{MC/MC}$ = 8.3 and 11.6 Å for PBO and PHO respectively. The shoulder close to Q_{II} could be attributed to intermolecular correlations (quite rare, in the view of the snapshot) or to some intramolecular correlations along the main chains. We note that amorphous PEO shows its main peak also in this Q-region.
- The SG/SG correlations display two clear main peaks centered around $Q_I^{SG/SG} \approx Q_I^{MC/MC} \approx Q_I$ and $Q_{II}^{SG/SG} \approx Q_{II}$, and a third broad feature is present around Q_{III}. We invoke the above arguments to assign a SG/SG intermolecular origin to the peak at $Q_{II}^{SG/SG}$. Interestingly, the finding of a peak in the SG/SG correlations around Q_I is the clear signature of the existence of side-group nanodomains, the average separation among which would be the same as that found for the main chains.
- The most striking feature is found in the cross-correlations MC/SG, that show a main negative peak practically mirroring the first peak of the MC/MC correlations. This negative peak reveals a strong anticorrelation between both substructures in the associated length scale ($2\pi/Q_I$). At Q-values larger than ≈1.2 Å^{-1} the MC/SG correlations practically vanish.

This analysis allows a clear identification of the origin of the peaks in the total structure factor:

- Peak II is practically dominated by SG/SG correlations.
- Peak I is the result of positive MC/MC and SG/SG correlations (the former being about twice as intense as the latter) and the strong negative MC/SG peak. The three contributions almost cancel each other, mainly for PBO, where peak I appears only as a shoulder. We note that as result of such superposition of contributions, the maximum of peak I in the total structure factor of PHO—where it can be better resolved—does not exactly correspond to the position of MC/MC and SG/SG peaks, but it is slightly shifted toward lower Q-values (from ≈0.54 Å^{-1} to ≈0.48 Å^{-1}). Thus, somewhat larger domain sizes are deduced from the examination of the total structure factor than the actual ones (about 10% in this case).
- To peak III, all correlations contribute positively. In fact, this peak is universally found in polymers and can be attributed to intramolecular correlations.[1] With increasing n_C, the relative weight of the SG/SG contribution naturally increases since a larger fraction of atoms are located along the side-group.

The two main differences between PBO and PHO partial structure factors concern only the first peak: its position is shifted toward lower Q-values and its intensity is increased in PHO with respect to PBO, signatures of bigger domain size and a more developed segregation of the molecular substructures. We note finally that the large contribution of the anticorrelation peak to the structure factor at low Q-values might hamper a precise determination of the nanodomains' sizes and consequently, probably also of their thermal evolution. We speculate that this could be the reason why different values for the expansion coefficient are deduced from the position of the peaks and from macroscopic measurements. Temperature-dependent MD-simulations—beyond the scope of this work—would be needed to explain the factor of 3 mismatch found in the experiments.

Once we have deciphered the structural details and the different contributions to the structure factor in PAOs, we can ask what would be the experimental observables delivered by such structures. Figure 12 shows what are the expectations for neutron diffraction experiments on differently h/d labeled samples calculated from the simulations by using eq 1 with the proper scattering lengths. In addition to the fully deuterated and fully protonated samples above-described, we have considered the cases of protonated main chains (hMC) and deuterated side groups (dSG) and vice versa (dMC and hSG), that in principle would be possible to synthesize. Deuterating a given molecular group enhances the corresponding correlations with respect to the hydrogenated material. For example, in both samples with deuterated side groups peak II—arising almost exclusively from SG/SG correlations—is extremely pronounced. The most spectacular effect nevertheless is achieved by deuterating only the main chains. Then, three factors give rise to the observation of basically only an isolated peak I: (i) the above-mentioned larger weight of the correlations of the deuterated subgroups; (ii) the average length density of the side groups becomes very small, leading to a suppression of peak II (though also of the smaller contribution to peak I) and, more important, (iii) due to the negative scattering length of H, the cross-correlations involving SG and MC atoms change sign and the strong negative MC/SG peak at Q_I is now positively added. As a result, the interdomain correlations are nicely reflected in the cross-section of such labeled samples.

■ CONCLUSIONS

The structure factors revealed by neutron diffraction on deuterated PAOs show basically the same features as those of PnMAs and thereby can also be interpreted assuming nanosegregation of main chains and side groups. Because of the chemical composition of the side groups (different from that of the main chains) the nanodomains should be PE-like structures. Thus, their characteristic structure should feature the signatures of the structure factor in PE, which is different from that of the main chains. By demanding the qualitative similarity with the structure factor of pure PE we have defined a soft criterion for the existence of nanodomains. Figure 4 illustrates that for PnMAs with n_C = 2 the resemblance is not yet there,

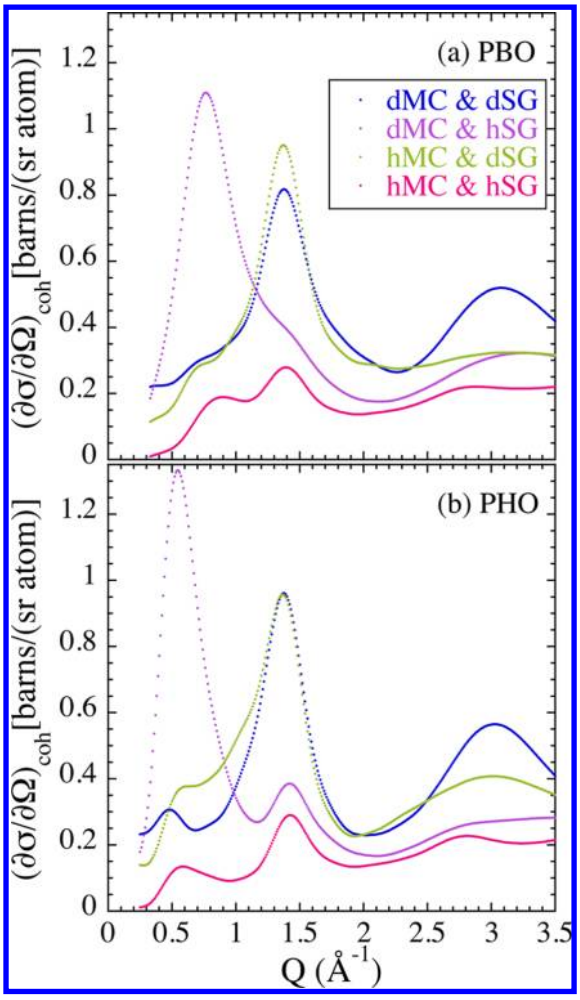

Figure 12. Coherent scattering cross sections calculated from the MD-simulations for the different deuteration labels indicated: (a) PBO; (b) PHO.

while for longer side groups we observe strong similarities with the structure factor of PE. For PAOs, this appears to be the case already for PBO (n_C = 2). Comparison with semicrystalline PE data here reported also shows that the local structure within the alkyl nanodomains in PAOs is more similar to bulk PE than in the PnMAs.

Furthermore, the diffraction data on both deuterated and protonated samples have provided a demanding test to validate our fully atomistic MD-simulations on PBO and PHO. These have been exploited to reveal the origin of the structure factor peaks, confirming the nanosegregation scenario. Thus, the lack of observation of confinement effects in the side-group dynamics of PAOs has to be attributed to other ingredients than the absence of structurally segregated phases. Large main-chain flexibility leading to similar characteristic times for the dynamics of side groups and main chains could be invoked to rationalize the different dynamical behavior in PAOs with respect to PnMAs.

AUTHOR INFORMATION

Corresponding Author

*E-mail: (G.J.S.) g.j.schneider@fz-juelich.de; (A.A.) a.arbe@ehu.es.

Notes

The authors declare no competing financial interest.

ACKNOWLEDGMENTS

We thank support by the "Donostia International Physics Center", the European Commission NoE SoftComp, Contract NMP3-CT-2004-502235, FP7-PEOPLE-2007-1-1-ITN (DYNACOP, EU), the projects MAT2007-63681, IT-436-07 (GV), and the Spanish Ministerio de Educacion y Ciencia (Grant No. CSD2006-53). C.G. acknowledges financial support by the International Helmholtz Research School on Biophysics and Soft Matter (IHRS BioSoft).

REFERENCES

(1) Frick, B.; Richter, D.; Ritter, C. *Europhys. Lett.* **1989**, *9*, 557.
(2) Alvarez, F.; Colmenero, J.; Zorn, R.; Willner, L.; Richter, D. *Macromolecules* **2003**, *36*, 238.
(3) Wind, M.; Graf, R.; Renker, S.; Spiess, H.; Steffen, W. *J. Chem. Phys.* **2005**, *122*, 014906.
(4) Genix, A.-C.; Arbe, A.; Alvarez, F.; Colmenero, J.; Schweika, W.; Richter, D. *Macromolecules* **2006**, *45*, 2522.
(5) Eilhard, J.; Zirkel, A.; Tschop, W.; Hahn, O.; Kremer, K.; Schärpf, O.; Richter, D.; Buchenau, U. *J. Chem. Phys.* **1999**, *110*, 1819.
(6) Genix, A.-C.; Arbe, A.; Alvarez, F.; Colmenero, J.; Schweika, W.; Richter, D. *Macromolecules* **2006**, *39*, 3947.
(7) Narros, A.; Arbe, A.; Alvarez, F.; Colmenero, J.; Zorn, R.; Schweika, W.; Richter, D. *Macromolecules* **2005**, *38*, 9847.
(8) Tyagi, M.; Arbe, A.; Alvarez, F.; J., C.; Gonzalez, M. A. *J. Chem. Phys.* **2008**, *129*, 224903.
(9) Perez-Aparicio, R.; Arbe, A.; Alvarez, F.; Colmenero, J.; Willner, L. *Macromolecules* **2009**, *42*, 8271.
(10) Gkourmpis, T.; Mitchell, G. *Macromolecules* **2011**, *44*, 3140.
(11) Heijboer, J. In *Physics of Non-Crystalline Solids*; Prins, J., Ed.; North-Holland: Amsterdam, 1965; p 231.
(12) McCrum, N.; Read, B.; Williams, G. *Anelastic, Dielectric Effects in Polymeric Solids*; Wiley: London, 1967.
(13) Cowie, J. *J. Macromol. Sci.—Phys. B* **1980**, *18*, 569.
(14) Meier, G.; Fytas, G.; Dorfmüller, T. *Macromolecules* **1984**, *17*, 957.
(15) Giebel, L.; Meier, G.; Fytas, G.; Fischer, E. W. *J. Polym. Sci., B: Polym. Phys.* **1992**, *30*, 1291.
(16) Garwe, F.; Schönhals, A.; Lockwenz, H.; Beiner, M.; Schröter, K.; Donth, E. *Macromolecules* **1996**, *29*, 247.
(17) Schröter, K.; Unger, R.; Reissig, S.; Garwe, F.; Kahle, S.; Beiner, M.; Donth, E. *Macromolecules* **1998**, *31*, 8966.
(18) Floudas, G.; Stepanek, P. *Macromolecules* **1998**, *31*, 6951.
(19) Beiner, M.; Schröter, K.; Hempel, E.; Reissig, S.; Donth, E. *Macromolecules* **1999**, *32*, 6278.
(20) Dudognon, E.; Bernès, A.; Lacabanne, C. *Macromolecules* **2001**, *34*, 3988.
(21) Dudognon, E.; Bernès, A.; Lacabanne, C. *Macromolecules* **2002**, *35*, 5927.
(22) Beiner, M. *Macromol. Rapid Commun.* **2001**, *22*, 869.
(23) Beiner, M.; Kabisch, O.; Reichl, S.; Huth, H. *J. Non-Cryst. Sol.* **2002**, *307*, 658.
(24) Hempel, E.; Beiner, M.; Huth, H.; Donth, E. *Thermochim. Acta* **2002**, *391*, 219.
(25) Pascui, O.; Beiner, M.; Reichert, D. *Macromolecules* **2003**.
(26) Beiner, M.; H., H. *Nat. Mater.* **2003**, *2*, 595.
(27) Hiller, S.; Pascui, O.; Kabisch, O.; Reichert, D.; Beiner, M. *New J. Phys.* **2004**, *6*, 1.
(28) Menissez, C.; Sixou, B.; David, L.; Vigier, G. *J. Non-Cryst. Sol.* **2005**, *351*, 595.
(29) Beiner, M. In *CP832, Flow Dynamics, The Second International Conference on Flow Dynamics*; Tokuyama, M., Maruyama, S., Eds.; American Institute of Physics: Melville, NY, 2006; p 134.
(30) Arbe, A.; Genix, A.-C.; Colmenero, J.; Richter, D.; Fouquet, P. *Soft Matter* **2008**, *4*, 1792.
(31) Arbe, A.; Genix, A.-C.; Arrese-Igor, S.; Colmenero, J.; Richter, D. *Macromolecules* **2010**, *43*, 3107.

(32) Gaborieau, M.; Graf, R.; Kahle, S.; Pakula, T.; H.W., S. *Macromolecules* **2007**, *40*, 6249.
(33) Cowie, J.; Haq, Z.; McEwen, I.; Velickovic, J. *Polymer* **1981**, *22*, 327.
(34) Arrighi, V.; Triolo, A.; McEwen, I. J.; Holmes, P.; Triolo, R.; Amenitsch, H. *Macromolecules* **2000**, *33*, 4989.
(35) Genix, A.-C.; Lauprêtre, F. *Macromolecules* **2005**, *38*, 2786.
(36) Gerstl, C.; Schneider, G. J.; Pyckhout-Hintzen, W.; Allgaier, J.; Willbold, S.; Hofmann, D.; Disko, U.; Frielinghaus, H.; Richter, D. *Macromolecules* **2011**, *44*, 6077.
(37) Gerstl, C.; Schneider, G. J.; Pyckhout-Hintzen, W.; Allgaier, J.; Richter, D.; Alegría, A.; Colmenero, J. *Macromolecules* **2010**, *43*, 4968.
(38) Gerstl, C.; Schneider, G. J.; Fuxman, A.; Zamponi, M.; Frick, B.; Seydel, T.; Koza, M.; Genix, A.-C.; Allgaier, J.; Richter, D.; Colmenero, J.; Arbe, A. *Macromolecules* **2012**, *45*, 4394.
(39) Moreno, A.; Arbe, A.; Colmenero, J. *Macromolecules* **2011**, *44*, 1695.
(40) Allgaier, J.; Willbold, S.; Chang, T. *Macromolecules* **2007**, *40*, 518.
(41) Springer, T. Quasielastic Neutron Scattering for the Investigation of Diffusive Motions in Solids, Liquids. In *Quasielastic Neutron Scattering for the Investigation of Diffusive Motions in Solids, Liquids*; Springer-Verlag: Berlin, Heidelberg, Germany, and New York, 1972; Vol. *64*.
(42) Lovesey, S. W. *Theory of Neutron Scattering from Condensed Matter*; Clarendon Press: Oxford, U.K., 1984.
(43) Bée, M. *Quasielastic Neutron Scattering*; Adam Hilger: Bristol, U.K., 1988.
(44) Squires, G. L. *Introduction to the Theory of Thermal Neutron Scattering*; Dover Publication Inc.: New York, 1996.
(45) Moon, R. M.; Riste, T.; Koehler, W. C. *Phys. Rev.* **1969**, *181*, 920.
(46) Schärpf, O. *Physica B: Condens. Matter* **1992**, *182*, 376.
(47) Theodorou, D.; Suter, U. *Macromolecules* **1986**, *19*, 139.
(48) Theodorou, D.; Suter, U. *Macromolecules* **1986**, *19*, 379.
(49) Arbe, A.; Colmenero, J. *Phys. Rev. E* **2009**, *80*, 041805.
(50) Carlsson, P.; Swenson, J.; Börjesson, L.; Torell, L.; McGreevy, R.; Howells, W. S. *J. Chem. Phys.* **1998**, *109*, 8719.
(51) Johnson, J.; Saboungi, M.-L.; Price, D.; Ansell, S.; Russell, T.; Halley, J.; Nielsen, B. *J. Chem. Phys.* **1998**, *109*, 7005.
(52) Arbe, A.; Genix, A.-C.; Arrese-Igor, S.; Colmenero, J.; Richter, D. *Macromolecules* **2010**, *43*, 3107.